Electrochemical Hydrogen Evolution on Ni_2P: Insights from Constant-Potential DFT and Microkinetic Modelling

Syam Sadan[a], Sander Øglænd Hanslin[b], Ingeborg-Helene Svenum[c], and Jaakko Akola*[a,d]

[a] *Department of Physics, Norwegian University of Science and Technology (NTNU), NO-7491 Trondheim, Norway*
[b] *Department of Physics, Technical University of Denmark (DTU), DK-2800 Kgs. Lyngby, Denmark*
[c] *SINTEF Industry, P.O. Box 4760 Torgarden, NO-7465 Trondheim, Norway*
[d] *Computational Physics Laboratory, Tampere University, FI-33101 Tampere, Finland*

S1 Methods

S1.1 Implicit Solvent Model

In the implicit description as detailed in [1,2], the solvent is represented as a polarisable dielectric medium surrounding the solute. The formalism is reiterated below for completeness of discussion.

The relative permittivity $\epsilon(n)$ is expressed as a functional of the solute electron density $n(\vec{r})$:

$$\epsilon(n(\vec{r})) = 1 + (\epsilon_\mathrm{b} - 1)S(n(\vec{r})), \tag{S1}$$

where ϵ_b is the bulk dielectric constant of the solvent. The smooth shape function $S(n)$ distinguishes between solute, cavity, and solvent regions:

$$S(n(\vec{r})) = \frac{1}{2}\,\mathrm{erfc}\left\{\frac{\log(n/n_c)}{\sigma\sqrt{2}}\right\}. \tag{S2}$$

Here, n_c defines the electron density at the solute–solvent boundary and σ controls the sharpness of the transition.

The solute–solvent free energy includes electrostatic field energy, interactions between solvent ions and the electrostatic potential, cavitation, dispersion, and the entropy of the ions. Minimisation of this free energy with respect to $n(\vec{r})$ introduces an additional solvent potential V_solv into the Kohn–Sham Hamiltonian:

$$V_\mathrm{solv} = \frac{\delta\epsilon(n)}{\delta n}\frac{|\nabla\phi|^2}{8\pi} + \phi\frac{\delta\rho_\mathrm{ion}}{\delta n} + \tau\frac{\delta|\nabla S|}{\delta n} + k_B T\frac{\delta S_\mathrm{ion}}{\delta n}. \tag{S3}$$

Here, $\phi(\vec{r})$ is the electrostatic potential, ρ_ion the ionic charge density, τ the effective surface tension (including cavitation, repulsion, and dispersion), and S_ion the entropy of ion mixing.

Minimisation of the solute–solvent free energy with respect to $\phi(\vec{r})$ yields the linearised Poisson–Boltzmann (LPB) equation, which governs the electrostatic potential distribution in the system:

$$\nabla\cdot[\epsilon(n(\vec{r}))\nabla\phi] - \kappa^2\phi = -\rho_s, \tag{S4}$$

$$S[n(\vec{r})]\frac{1}{\lambda_D^2} = \kappa^2, \tag{S5}$$

$$\left(\frac{2c^0 z^2 e^2}{k_B T}\right) = \frac{1}{\lambda_D^2}, \tag{S6}$$

where ρ_s is the total solute charge density, λ_D the Debye length, c^0 the bulk ionic concentration, z the ionic valency, e the elementary charge, k_B Boltzmann's constant, and T the absolute temperature.

S1.2 Constant Potential Formalism

Electrochemical reactions occur at a fixed applied potential, whereas standard DFT operates at a fixed charge. To bridge this gap, energy differences were evaluated at constant potential using the grand canonical formalism. The grand canonical energy is obtained via a Legendre transformation of the Helmholtz free energy [3,4]:

$$\Omega(\mathrm{U}) = \mathrm{E}_\mathrm{elec}^\mathrm{DFT}(\mathrm{U}) - \delta\,\mathrm{q}_\mathrm{elec}(\mathrm{U})\mathrm{U} - \delta\,\mathrm{q}_\mathrm{elec}(\mathrm{U})\mathrm{V}_\mathrm{solv}, \tag{S7}$$

where $\mathrm{E}_\mathrm{elec}^\mathrm{DFT}$ is the DFT electronic energy, $\delta\mathrm{q}_\mathrm{elec}$ the electrode charge, U the applied potential and V_solv is the potential in the bulk solvent. The final term in Eq. (S7) is specific to the VASPSol implementation [1,2,5]. U and V_solv are relative to the vacuum scale. Expressed in terms of electron number change $\delta\mathrm{n}_\mathrm{e}$,

$$\Omega(\mathrm{U}) = \mathrm{E}_\mathrm{elec}^\mathrm{DFT}(\mathrm{U}) + \delta\mathrm{n}_\mathrm{e}(\mathrm{U})\,\mathrm{U} + \delta\mathrm{n}_\mathrm{e}(\mathrm{U})\mathrm{V}_\mathrm{solv}. \tag{S8}$$

*Corresponding author: jaakko.akola@tuni.fi

The potential is referenced to the standard hydrogen electrode (SHE) in vacuum scale,

$$\mathrm{U\ vs\ SHE} = \mathrm{U} - \mathrm{U}^{\mathrm{SHE}}, \quad \mathrm{U}^{\mathrm{SHE}} = 4.43\ \mathrm{V}, \tag{S9}$$

with $\mathrm{U} = -\mu_{\mathrm{e}}/|\mathrm{e}|$ defined by the electron chemical potential. In metallic systems μ_{e} equals the Fermi level and in solvent-inclusive calculations, U is shifted by the bulk solvent potential $\mathrm{V_{solv}}$:

$$\mathrm{U} = (-\epsilon_{\mathrm{F}}/|\mathrm{e}|) - \mathrm{V_{sol}}. \tag{S10}$$

Voltage scans are performed by varying the electron count $\delta\mathrm{n_e}$ in the simulation cell[4], giving

$$\mathrm{U\ vs\ SHE}(\delta\mathrm{n_e}) = \mathrm{U}(\delta\mathrm{n_e}) - \mathrm{U}^{\mathrm{SHE}}, \qquad \Omega(\mathrm{U}) = \mathrm{E}^{\mathrm{DFT}}_{\mathrm{elec}}(\mathrm{U}) + \delta\mathrm{n_e}(\mathrm{U})\,\mathrm{U} + \delta\mathrm{n_e}(\mathrm{U})\mathrm{V_{solv}} \tag{S11}$$

In practice, stabilisation occurs when $\delta\mathrm{n_e}$ and U have opposite signs, lowering Ω by $|\delta\mathrm{n_e U}|$. The electrode charge $\delta\mathrm{q_{elec}}(\mathrm{U})$ must be carefully monitored, since abrupt changes in electrode state can yield different values at the same U.

For small variations around a reference potential $\mathrm{U_0}$, the dependence of Ω can be approximated by a quadratic form,

$$\Omega(\mathrm{U}) \approx \mathrm{E}^{\mathrm{DFT}}_{\mathrm{elec}}(\mathrm{U_0}) - \tfrac{1}{2}\mathrm{C}\,[\mathrm{U} - \mathrm{U_0}]^2, \tag{S12}$$

where C is the capacitance, obtained from the curvature of the grand canonical energy profile.

S1.3 Microkinetic Model

The time evolution of the probability of occupying state i is described by the master equation,

$$\frac{\mathrm{dp_i}}{\mathrm{dt}} = \sum_{\mathrm{j,\,i\neq j}} \mathrm{k_{ij}p_j} - \mathrm{k_{ii}p_i}, \tag{S13}$$

where $\mathrm{k_{ij}}$ are the GC-TST rate constants,

$$\mathrm{k_{ij}} = \langle\kappa\rangle\,\frac{\mathrm{k_B T}}{\mathrm{h}}\exp\!\left(-\frac{\Omega^{\mathrm{ij}}_{\mathrm{a}}}{\mathrm{k_B T}}\right). \tag{S14}$$

Here, $\Omega^{\mathrm{ij}}_{\mathrm{a}}$ are the grand-canonical activation barriers for $\mathrm{j} \to \mathrm{i}$ transitions, and $\mathrm{k_{ii}} = \sum_{\mathrm{j}} \mathrm{k_{ji}}$ represents the total outflux from state i. The transmission coefficient $\langle\kappa\rangle$ is taken as unity.

When multiple pathways connect the same pair of states (e.g., $\mathrm{j} \to \mathrm{j}+1$ via forward Volmer or backward Heyrovsky), the larger of the competing rate constants is used in eq. (S13). The backward Heyrovsky and Tafel steps are set to zero to mimic low $\mathrm{H_2}$ concentrations and seamless diffusion. Volmer and Heyrovsky activation barriers are corrected by 0.2 eV to account for proton transfer and solvent reorganisation effects[6,7].

Equation (S13) can be written in matrix form,

$$\frac{\mathrm{dp}}{\mathrm{dt}} = \mathrm{K}\cdot\mathrm{p}, \tag{S15}$$

where p is an $\mathrm{N_s}\times 1$ column vector of state probabilities and K is the $\mathrm{N_s}\times\mathrm{N_s}$ transition matrix. The steady-state condition, $\mathrm{K}\cdot\mathrm{p} = 0$, yields the occupation probabilities $\mathrm{p_j}$.

The rate of an elementary transition $\mathrm{j} \to \mathrm{i}$ is then

$$\mathrm{r_{ij}} = \mathrm{k_{ij}}\cdot\mathrm{p_j}. \tag{S16}$$

Finally, the net current density j is given by

$$\mathrm{j} = \frac{-\mathrm{e}}{\mathrm{A}}\left(\mathrm{r_{v^+}} + \mathrm{r_{h^+}} - \mathrm{r_{v^-}}\right), \tag{S17}$$

where e is the elementary charge and A the surface area per adsorption site. The number of adsorption sites corresponds to the H-saturated surface: 4 for the pristine and 6 for the reconstructed termination. The simulation cell area normal to the z-axis is 119.29×10^{-16} $\mathrm{cm^2}$.

S1.4 Benchmark calculations

S1.4.1 Frozen transition state approximation

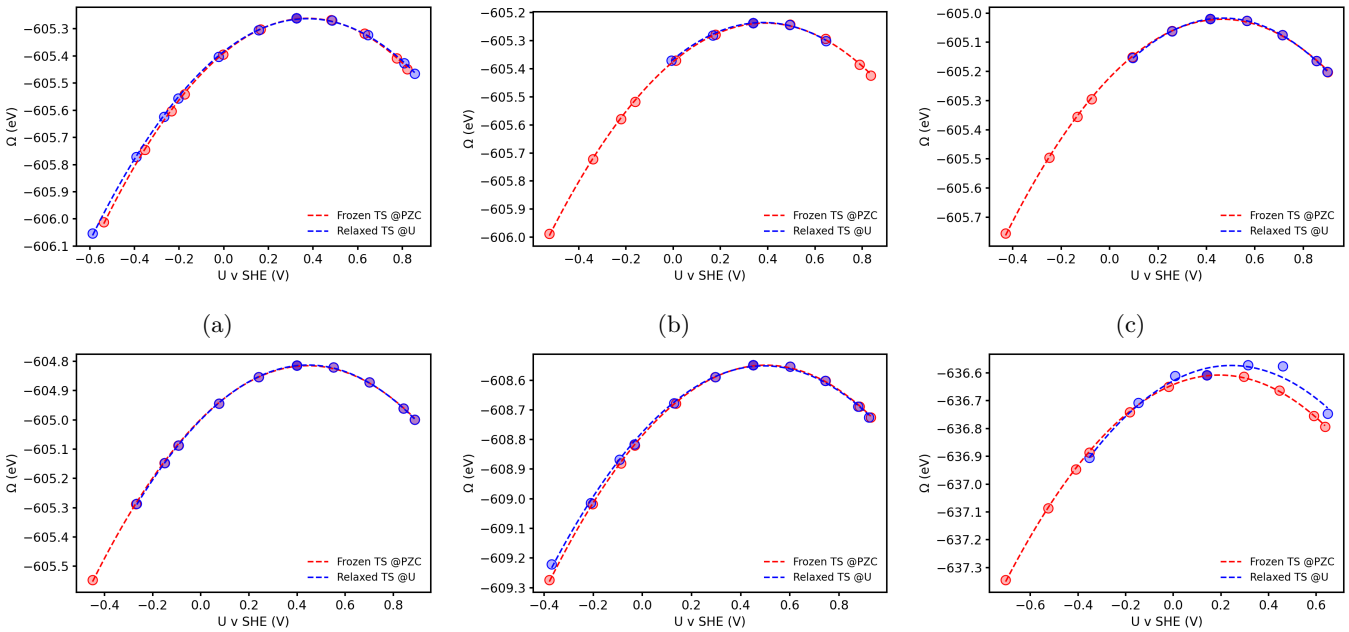

Figure S1: Grand canonical transition-state energies as a function of applied potential, comparing structures fixed at the potential of zero charge with structures relaxed separately at each potential. Comparisons include a) 4H0-5H0-Volmer b) 4H0-5H1-Volmer c) 5H0-3H0-Tafel-1 d) 5H0-3H0-Tafel-2 e) 5H0-4H0-Heyrovsky f) 6H0-7H1-Volmer.

S1.4.2 Influence of dipole interactions on activation energies

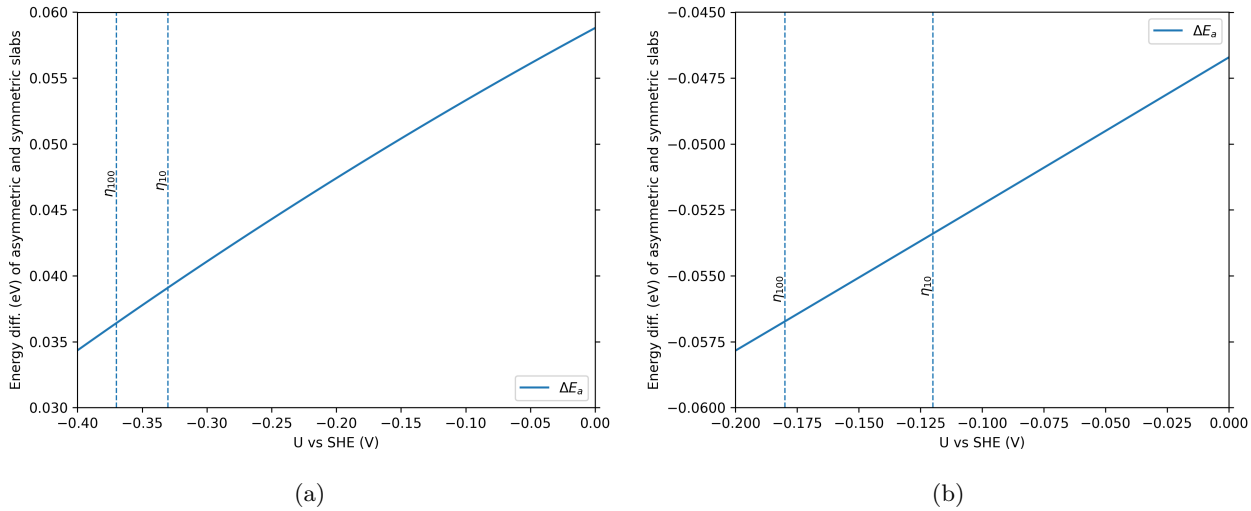

Figure S2: The difference between activation energies of asymmetrical and symmetrical HER systems on a) pristine (Ni_3P_2) and b) reconstructed (Ni_3P_2+4P) surface termination. In the relevant potential range, the activation energies from asymmetric slabs differ from the symmetric reference by at most 0.06 eV, being lower for the reconstructed case and higher for the pristine case. This assessment is based on Volmer-step benchmarks, and the impact of this sensitivity on the polarisation behaviour is discussed in Fig. S3.

S1.4.3 Polarisation sensitivity to activation energy

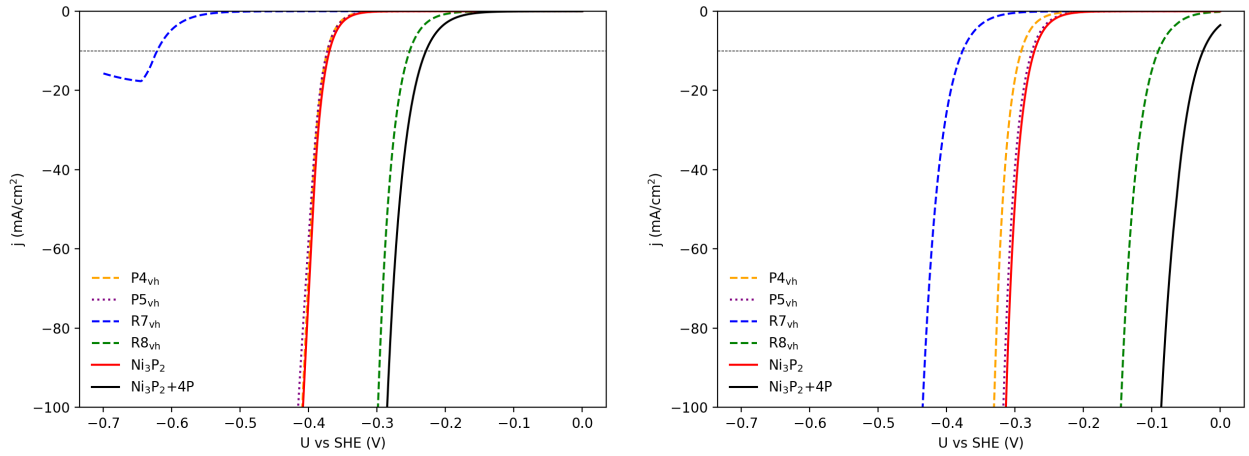

(a) (b)

Figure S3: Polarisation curves of HER on pristine (Ni_3P_2) and reconstructed (Ni_3P_2+4P) surfaces showing the effect of a ±0.06 eV change in activation energy with a) and a) corresponding to an increase and decrease of 0.06 eV, respectively. P/RX_{vh} stands for pristine/reconstructed surface Volmer-Heyrovsky cycles. The solid line represents the total current density, while dashed lines correspond to individual cycles. The orange ($P4_{vh}$) and purple ($P5_{vh}$) curves lie close to the red (Ni_3P_2) curve. A 0.06 eV reduction in the HER grand-canonical activation energy on the pristine surface lowers the overpotential by ∼60 mV across 10–100 mA cm^{-2} relative to the reported values, while a 0.06 eV increase on the reconstructed surface raises the overpotential by ∼110 mV over the same current-density range.

S1.5 Nernst conversion

The overpotential (vs RHE) values as reported for 10 and 100 mA cm^{-2} are 79 and 150 mV in[8], and 112 and 450 mV in[9], respectively. The E_{RHE} values obtained from the experiments[8,9] were converted to $E_{vs\ SHE}$ using the form (S18) derived from the Nernst equation.

$$E_{vs\ SHE}(V) = E_{vs\ RHE}(V) - (2.303RT/F) \cdot pH \tag{S18}$$

The details are available in Chapter 7, and specifically in section 7.2.7 (eq. 7.47b) of the reference[10]. The evolution of the pH correction term $-(2.303RT/F) \cdot pH$ in (S18), which is the potential of RHE vs SHE, is discussed in[11]. For 0.5 M H_2SO_4, the Nernst conversion equation assumes the form $E_{vs\ SHE}$ (V) = $E_{vs\ RHE}$ (V) - 0.017 (0.018) at 25 (40) °C. The pH is ∼ 0.29 for both cases. The pH of the solution used in the calculations considered the temperature dependence of K_2 of the form -RT ln(K_2) (J·mol^{-1}) = 57092.9 - 1724.98 T + 275.667 ln(T/K) T[12].

In the reference[13], $\eta_{20,\ vs\ RHE}$ = -130 mV and $\eta_{20,\ vs\ RHE}$ = -197 mV. However, the information on the temperature at which the electrochemical measurements are made is unavailable. Since a temperature change of 15 °C only changes the potential value by 1 mV, a correction corresponding to 25 °C is considered in this article. Hence, the corrected value would be $\eta_{20,\ vs\ SHE}$ = -147 mV and $\eta_{100,\ vs\ SHE}$ = -214 mV, respectively.

S2 Results

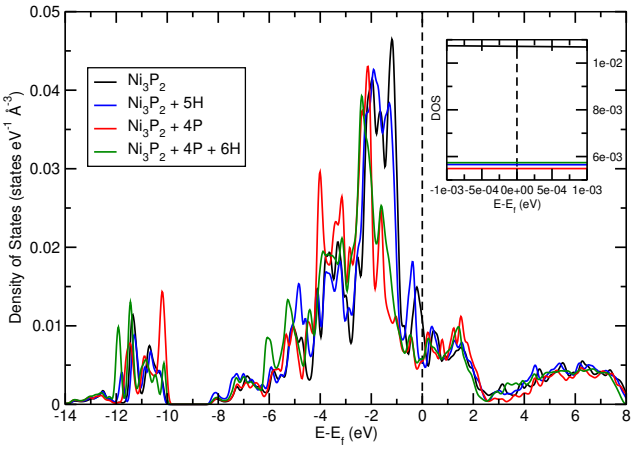

Figure S4: Density of states (DOS) of the 7-layer asymmetric Ni_3P_2 slab with pristine, reconstructed, and hydrogen-adsorbed surface terminations.

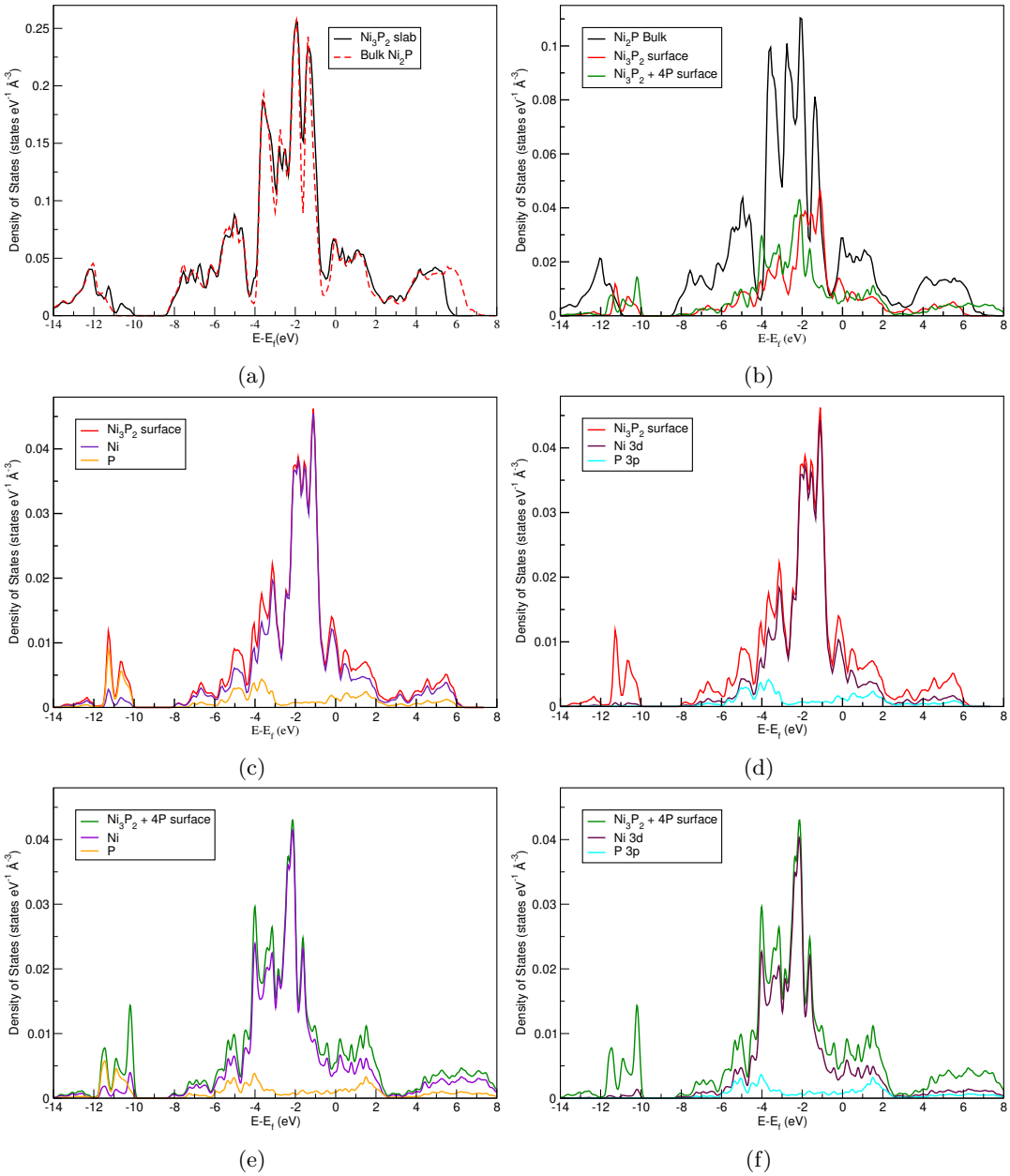

Figure S5: DOS of bulk Ni_2P and the pristine and reconstructed Ni_3P_2 surface terminations. Comparisons include (a) bulk and symmetric 15-layer slab, (b) bulk and asymmetric 7-layer pristine and reconstructed slabs, (c) surface atoms and (d) dominant orbitals of the pristine surface, and (e) surface atoms and (f) dominant orbitals of the reconstructed surface.

S2.1 Pristine Surfaces

S2.1.1 $P1_{vvt}$

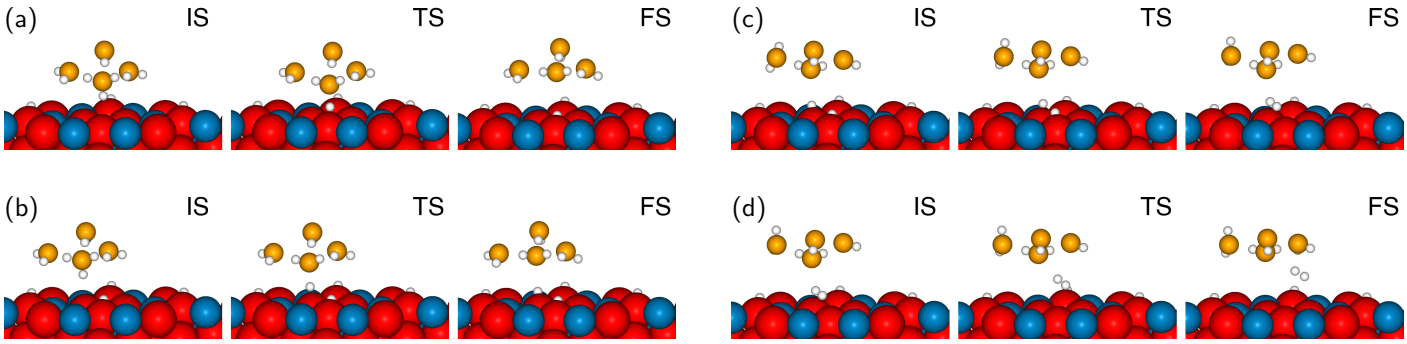

Figure S6: Hydrogen evolution via the $P1_{vvt}$ pathway on Ni_3P_2. IS, TS, and FS for Volmer steps (a) 3 to 4 and (b) 4 to 5 H coverages, and for (c) H_2 formation and (d) desorption via Tafel.

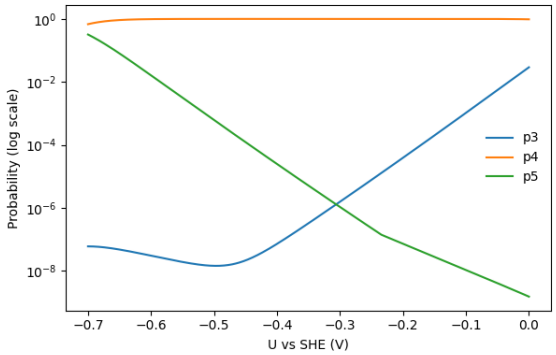

(a)

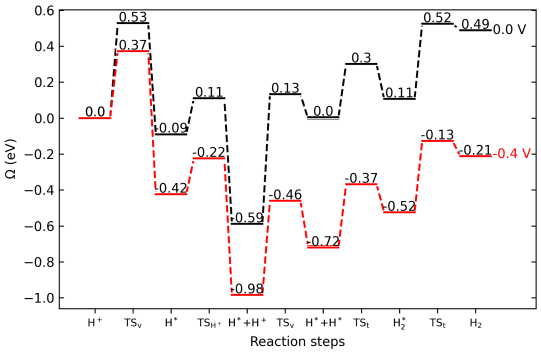

(d)

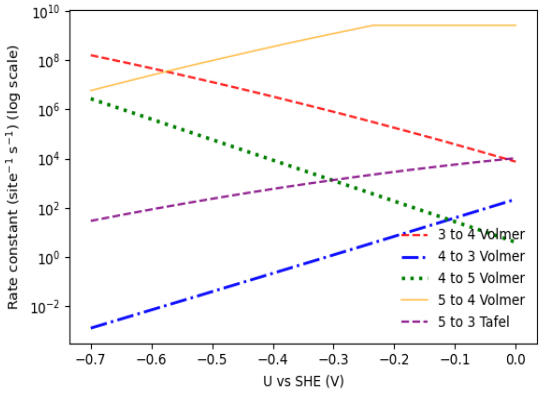

(b)

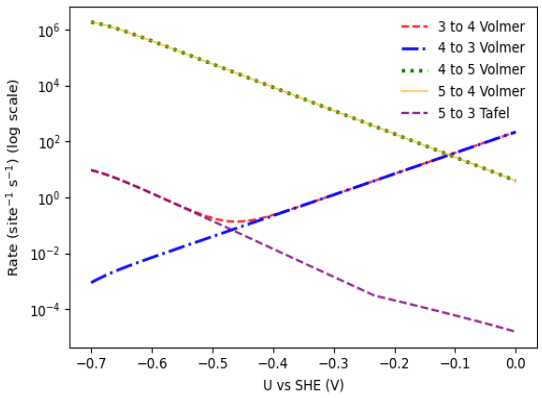

(c)

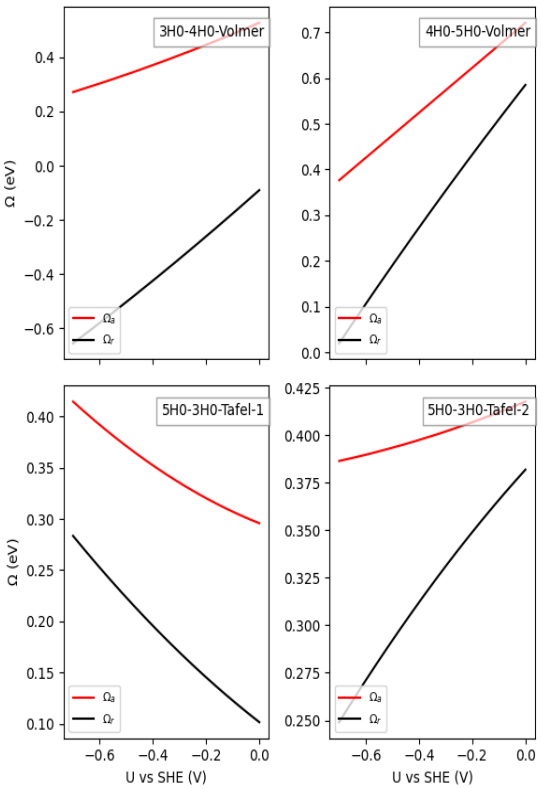

(e)

Figure S7: GC-TST and MKM results for $P1_{vvt}$. (a) pn - probability of nH state, (b) rate constants, (c) rates, (d) energy landscapes, (e) reaction and activation energies of elementary steps.

S2.1.2 $P2_{vvt}$

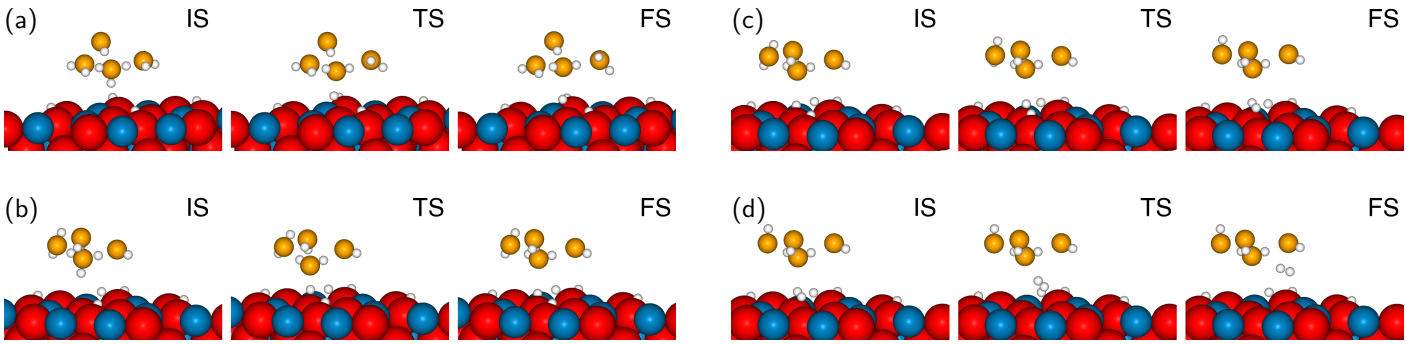

Figure S8: Hydrogen evolution via the $P2_{vvt}$ pathway on Ni_3P_2. IS, TS, and FS for Volmer steps (a) 4 to 5 and (b) 5 to 6 H coverages, and for (c) H_2 formation and (d) desorption via Tafel.

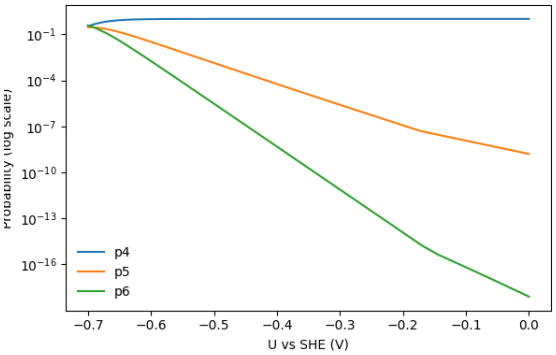

(a)

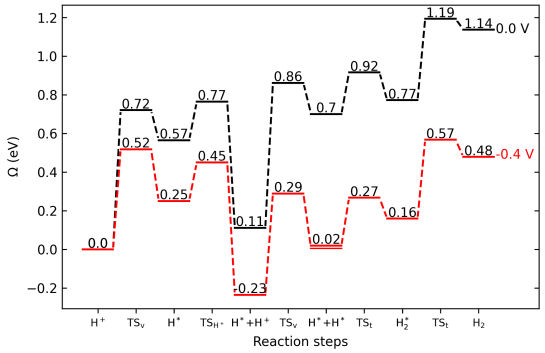

(d)

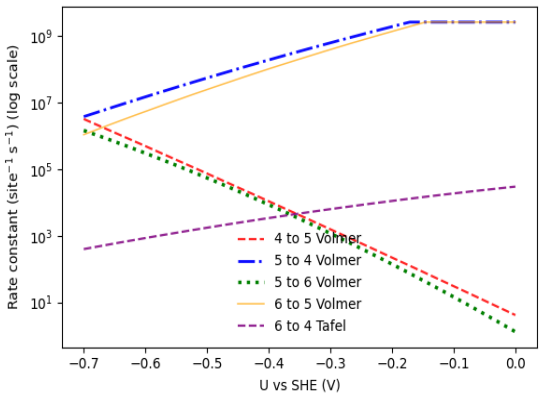

(b)

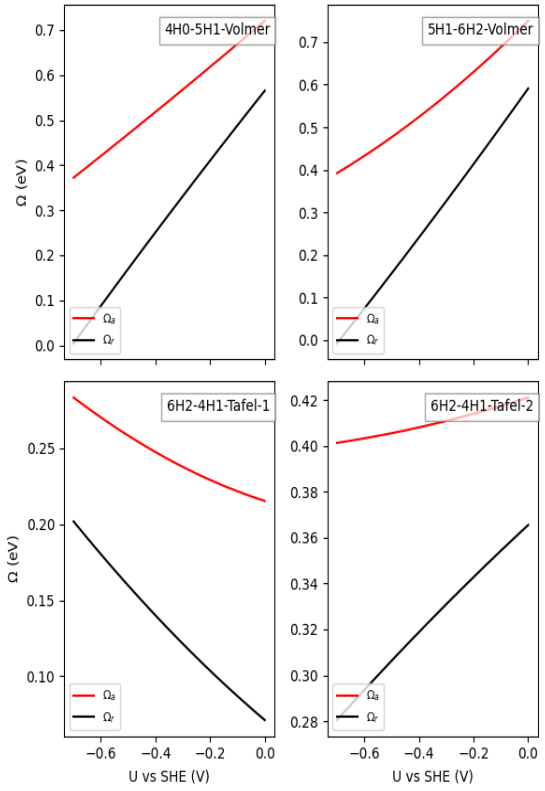

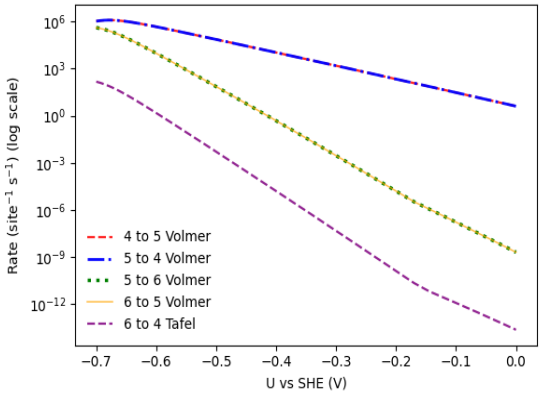

(c)

(e)

Figure S9: GC-TST and MKM results for $P2_{vvt}$. (a) pn - probability of nH state, (b) rate constants, (c) rates, (d) energy landscapes, (e) reaction and activation energies of elementary steps.

S2.1.3 $P3_{vvt}$

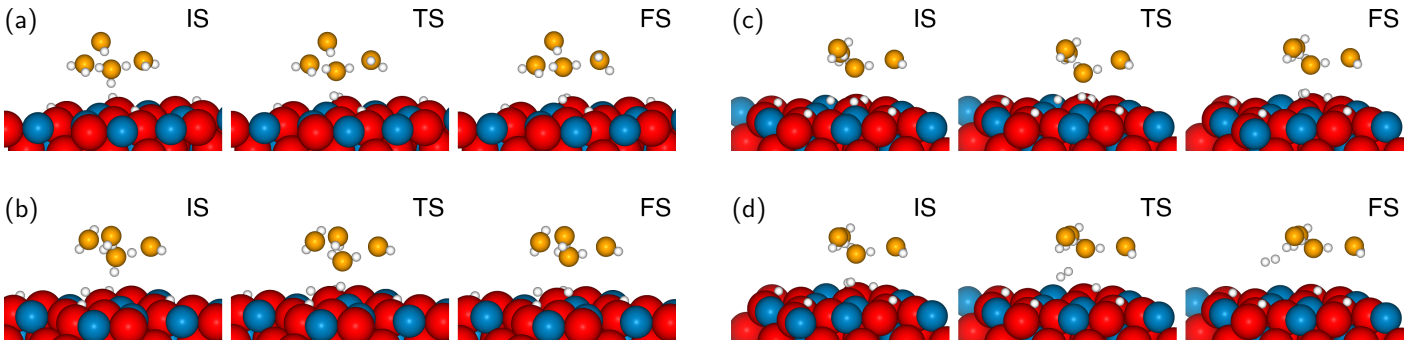

Figure S10: Hydrogen evolution via the $P3_{vvt}$ pathway on Ni_3P_2. IS, TS, and FS for Volmer steps (a) 4 to 5 and (b) 5 to 6 H coverages, and for (c) H_2 formation and (d) desorption via Tafel.

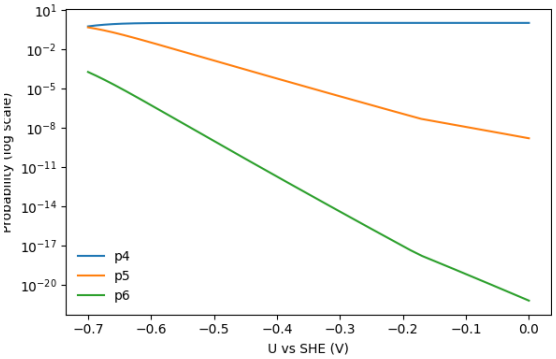

(a)

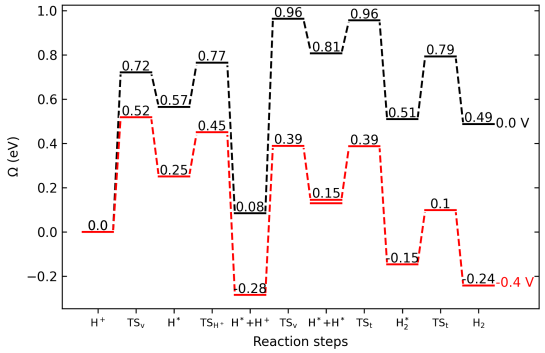

(d)

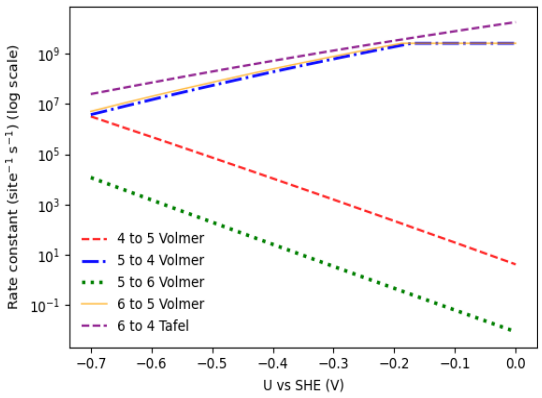

(b)

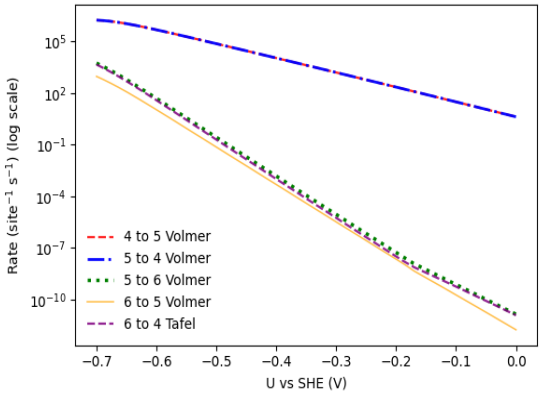

(c)

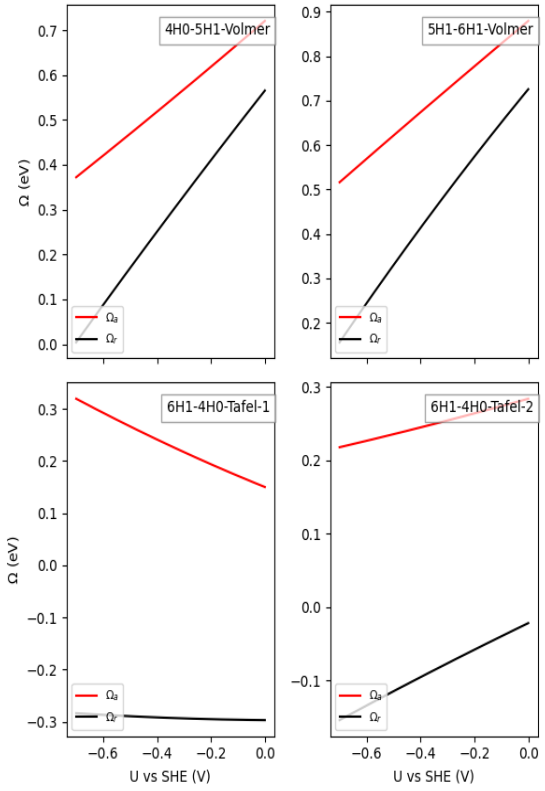

(e)

Figure S11: GC-TST and MKM results for $P3_{vvt}$. (a) pn - probability of nH state, (b) rate constants, (c) rates, (d) energy landscapes, (e) reaction and activation energies of elementary steps.

S2.1.4 $P4_{vh}$

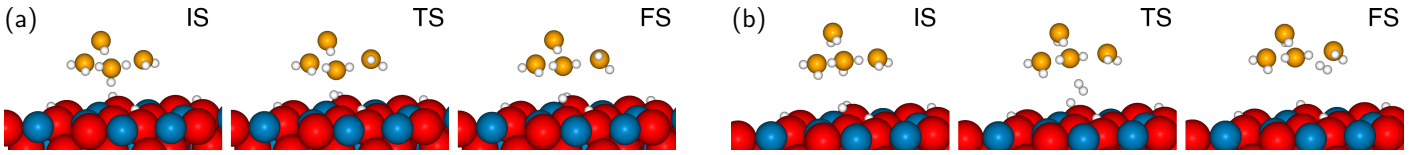

Figure S12: Hydrogen evolution via the $P4_{vh}$ pathway on Ni_3P_2. IS, TS, and FS for Volmer step (a) 4 to 5 and (b) H_2 evolution via Heyrovsky.

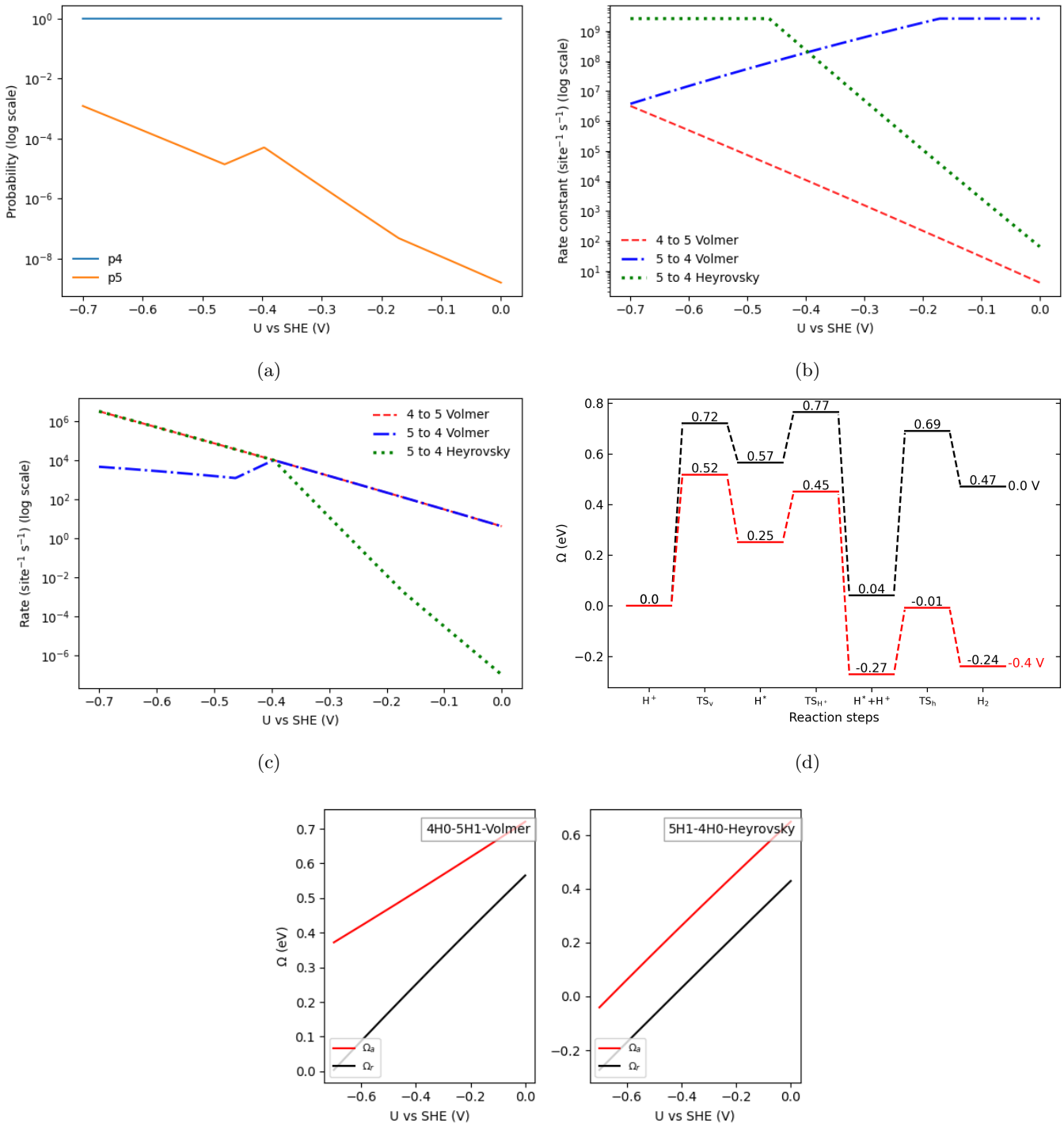

Figure S13: GC-TST and MKM results for $P4_{vh}$. (a) pn - probability of nH state, (b) rate constants, (c) rates, (d) energy landscapes, (e) reaction and activation energies of elementary steps.

S2.1.5 $P5_{vh}$

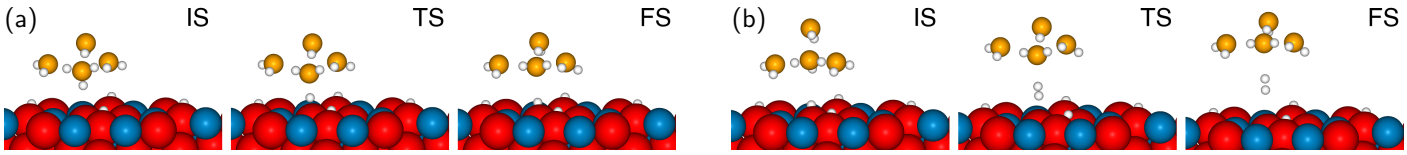

Figure S14: Hydrogen evolution via the $P5_{vh}$ pathway on Ni_3P_2. IS, TS, and FS for Volmer step (a) 4 to 5 and (b) H_2 evolution via Heyrovsky.

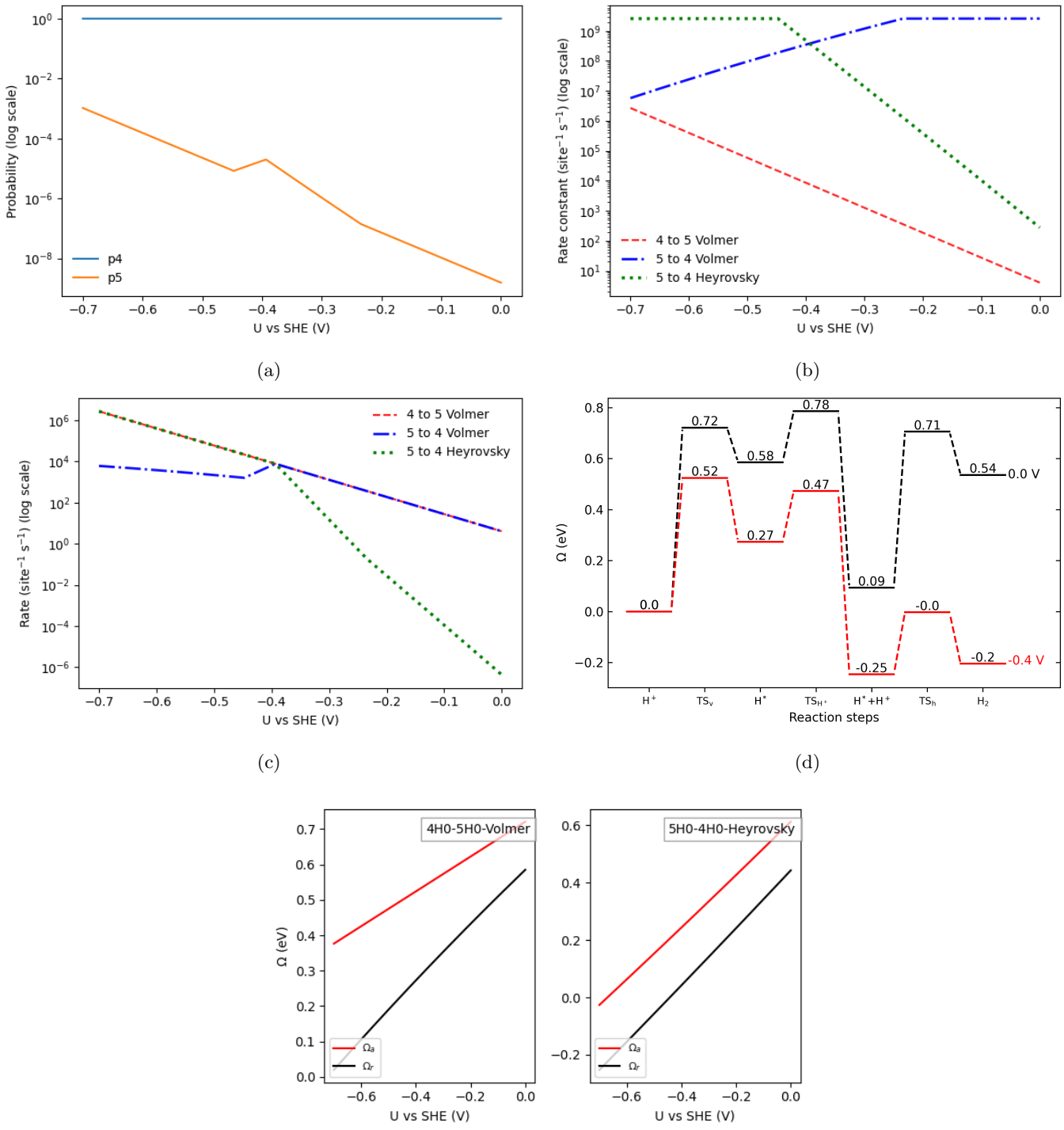

Figure S15: GC-TST and MKM results for $P5_{vh}$. (a) pn - probability of nH state, (b) rate constants, (c) rates, (d) energy landscapes, (e) reaction and activation energies of elementary steps.

S2.2 Reconstructed Surfaces

S2.2.1 $R6_{vvt}$

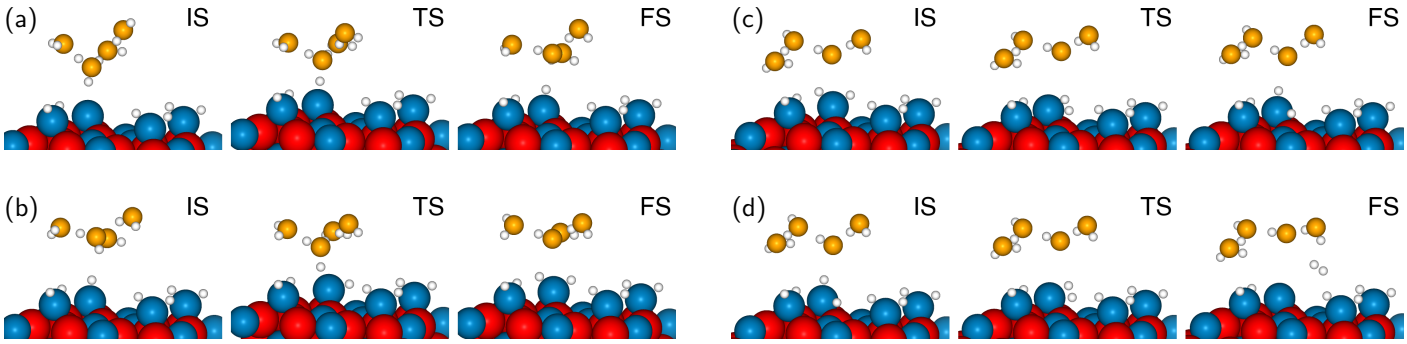

Figure S16: Hydrogen evolution via the $R6_{vvt}$ pathway on Ni_3P_2 + 4P. IS, TS, and FS for Volmer steps (a) 6 to 7 and (b) 7 to 8 H coverages, and for (c) H_2 formation and (d) desorption via Tafel.

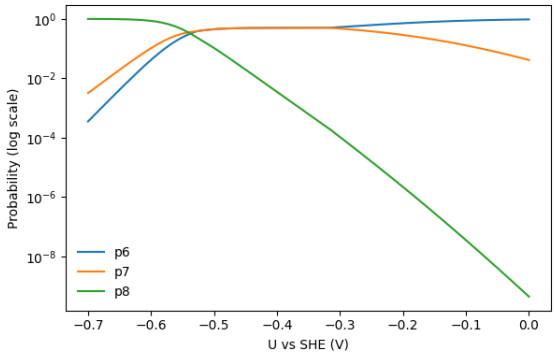

(a)

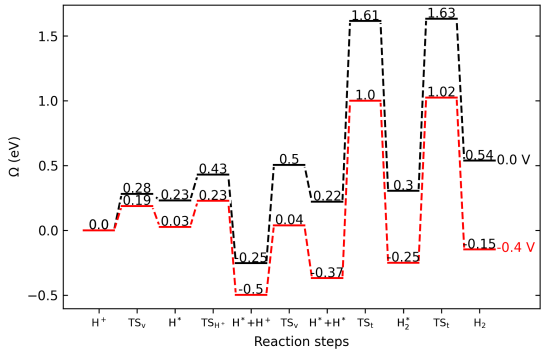

(d)

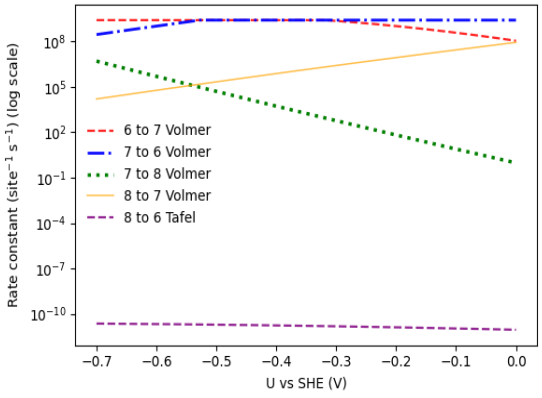

(b)

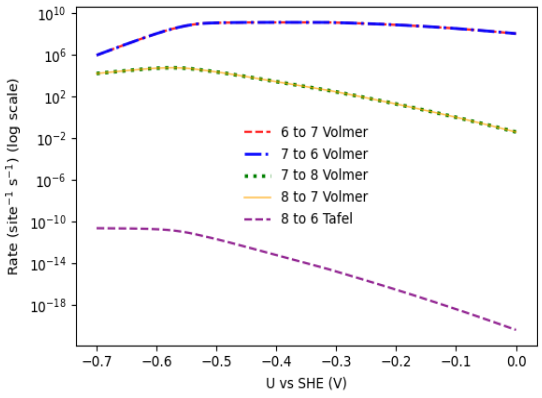

(c)

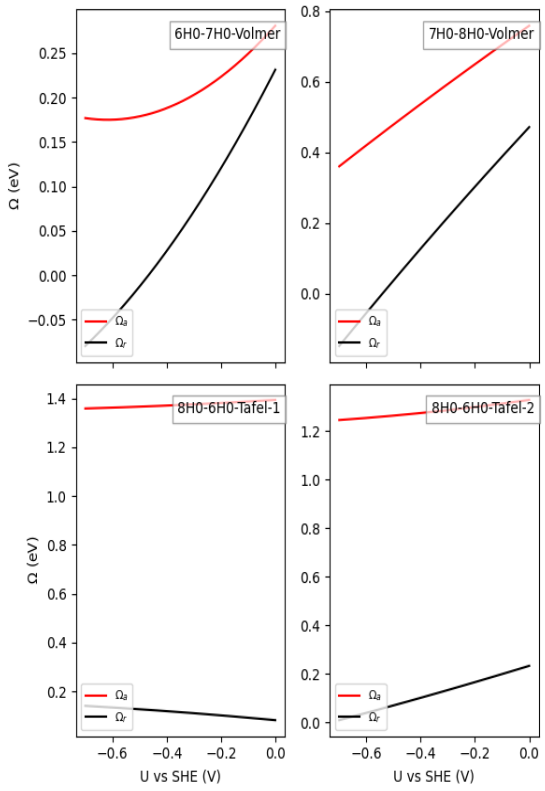

(e)

Figure S17: GC-TST and MKM results for $R6_{vvt}$. (a) pn - probability of nH state, (b) rate constants, (c) rates, (d) energy landscapes, (e) reaction and activation energies of elementary steps.

S2.2.2 $R7_{vh}$

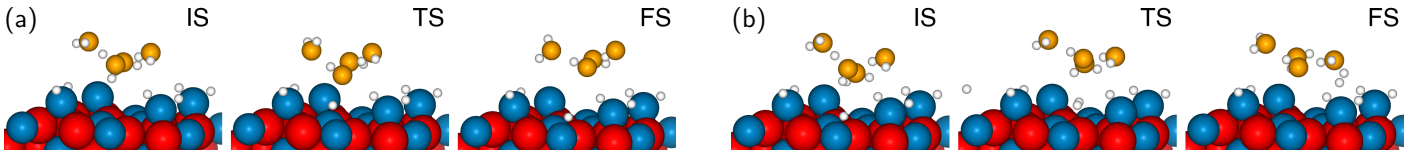

Figure S18: Hydrogen evolution via the $R7_{vh}$ pathway on Ni_3P_2 + 4P. IS, TS, and FS for Volmer step (a) 6 to 7 and (b) H_2 evolution via Heyrovsky.

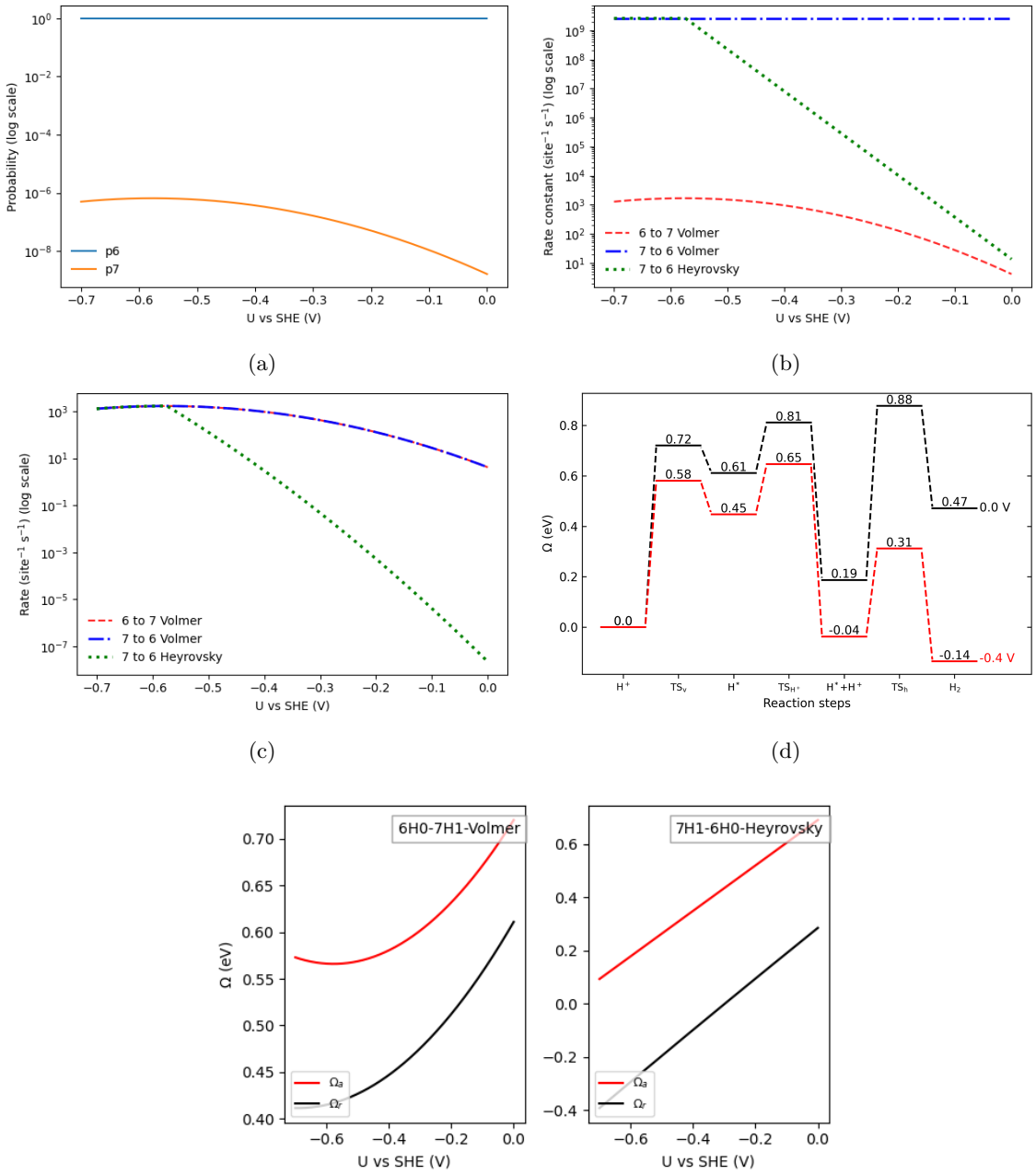

Figure S19: GC-TST and MKM results for $R7_{vh}$. (a) pn - probability of nH state, (b) rate constants, (c) rates, (d) energy landscapes, (e) reaction and activation energies of elementary steps.

S2.2.3 $R8_{vh}$

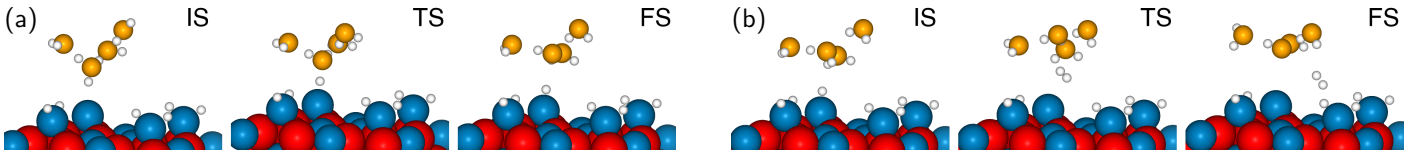

Figure S20: Hydrogen evolution via the $R8_{vh}$ pathway on Ni_3P_2 + 4P. IS, TS, and FS for Volmer step (a) 6 to 7 and (b) H_2 evolution via Heyrovsky.

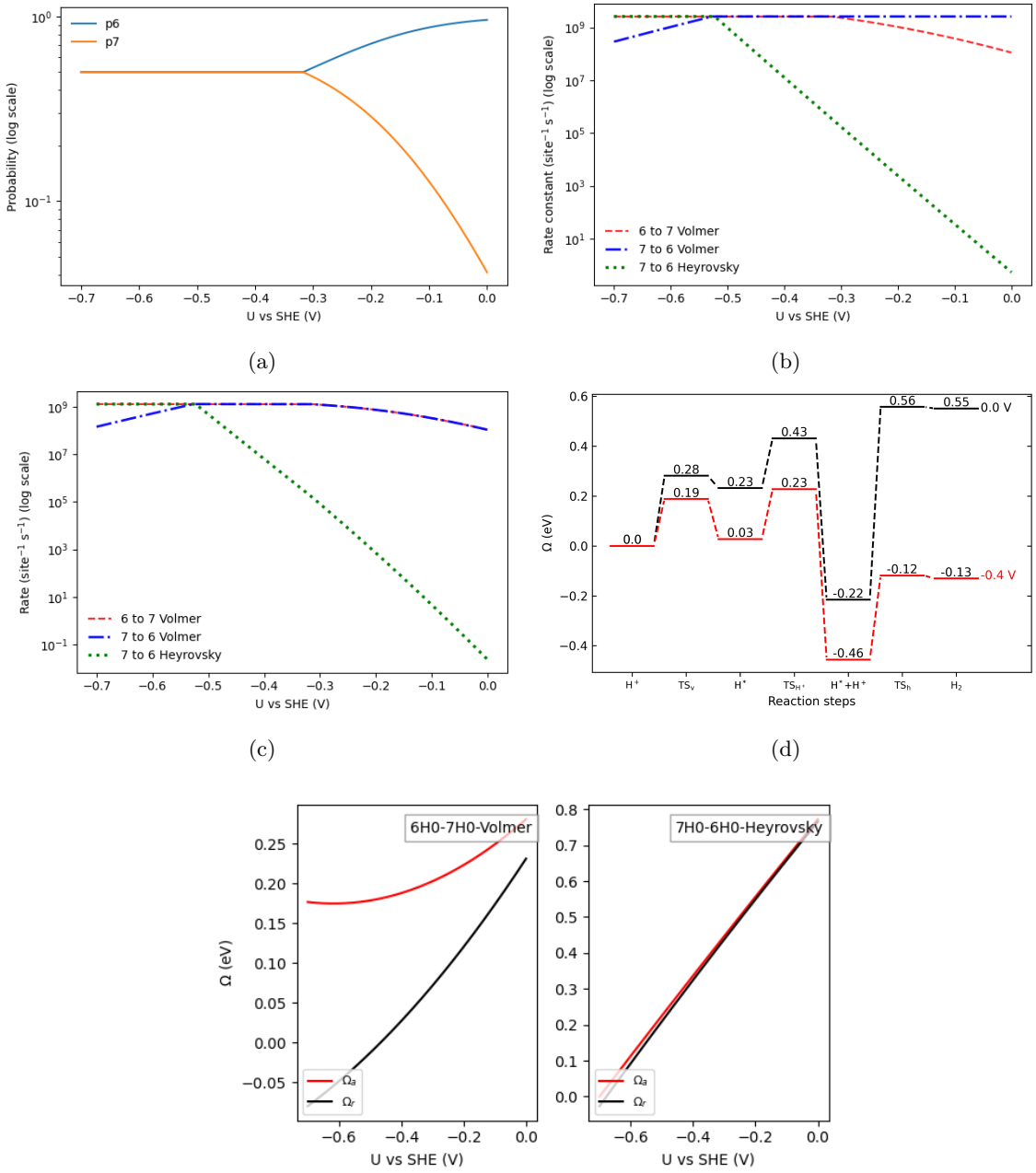

Figure S21: GC-TST and MKM results for $R8_{vh}$. (a) pn - probability of nH state, (b) rate constants, (c) rates, (d) energy landscapes, (e) reaction and activation energies of elementary steps.

S2.2.4 Full-network microkinetic model

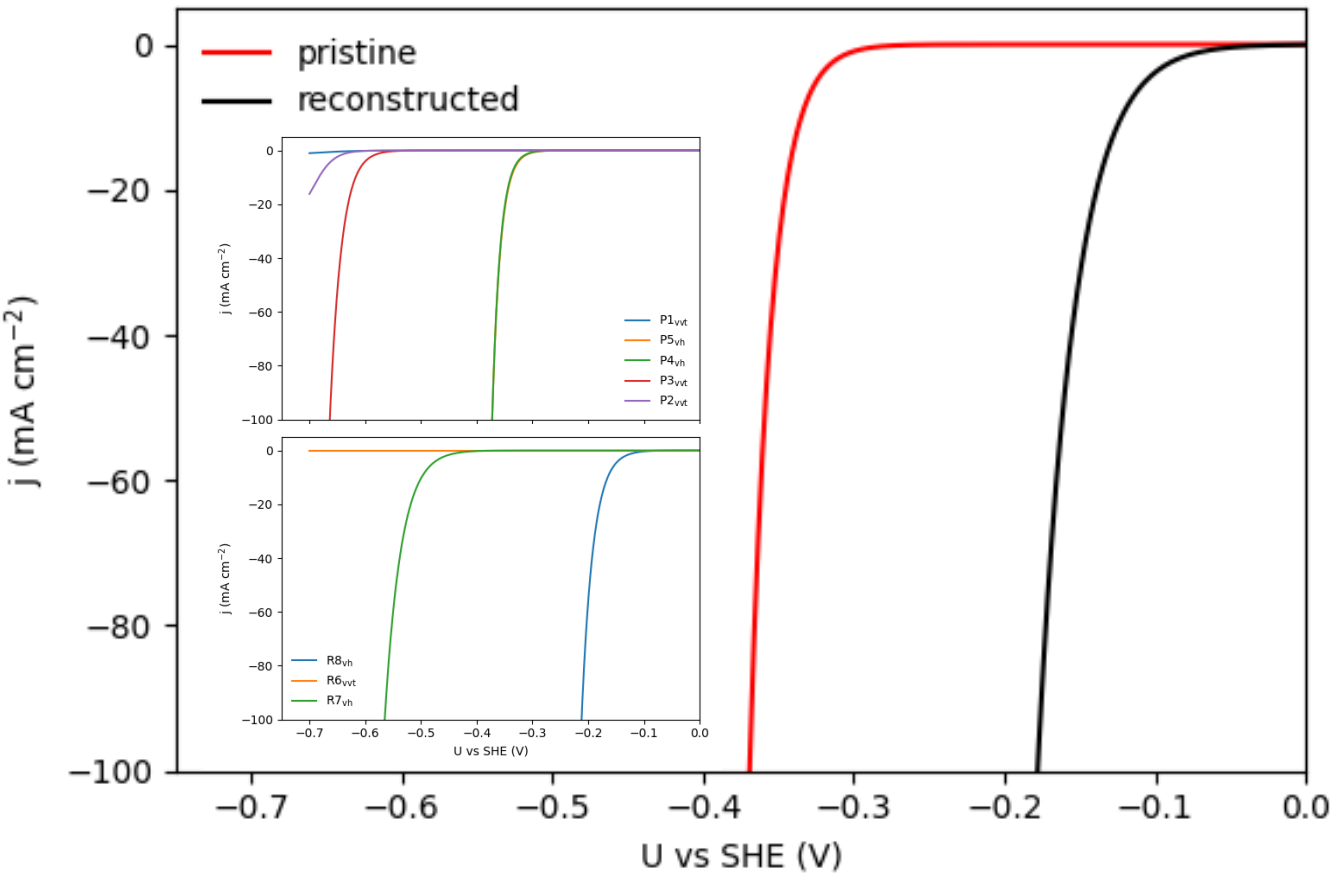

Figure S22: Polarisation curve of pristine and reconstructed surface terminations: pristine (red) and reconstructed (black). The insets show individual cycles for pristine (top) and reconstructed (bottom) surface terminations.

Table 1: Overpotential values (in mV) at different current densities across cycles. PC refers to Polycrystalline.

Ni_2P-surface/Cycle	**Overpotential in mV (vs SHE)**		
	η_{10}	η_{20}	η_{100}
pristine (Ni_3P_2)	330	345	370
reconstructed (Ni_3P_2+P)	120	139	180
$Ni_2P(001)$ [13]	–	147	214
$Ni_2P(001)$ [14]	–	–	343 ± 22
$Ni_2P(111)$ [8]	96	–	∼167
$Ni_2P(PC)$ [9]	130	–	468
P5$_{vh}$ (4H0–5H0–4H0)	340	–	370
P4$_{vh}$ (4H0–5H1–4H0)	340	–	370
P3$_{vvt}$ (4H0–5H1–6H1–4H0)	620	–	660
P2$_{vvt}$ (4H0–5H1–6H2–4H1)	680	–	–
R8$_{vh}$ (6H0–7H0–6H0)	160	–	210
R7$_{vh}$ (6H0–7H1–6H0)	500	–	570

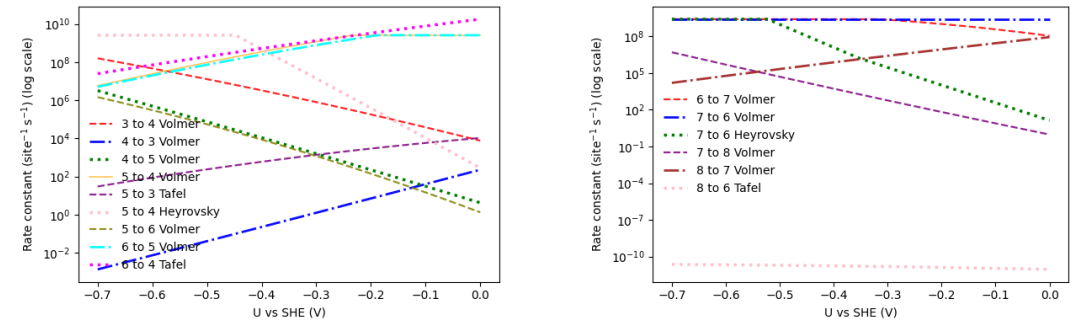

(a)

(b)

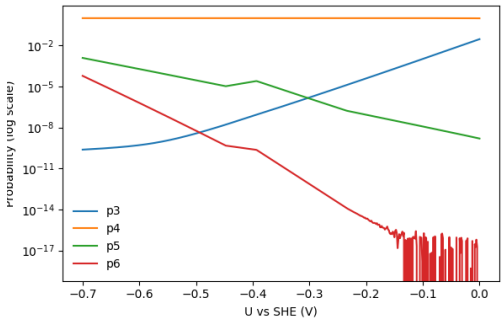

(c)

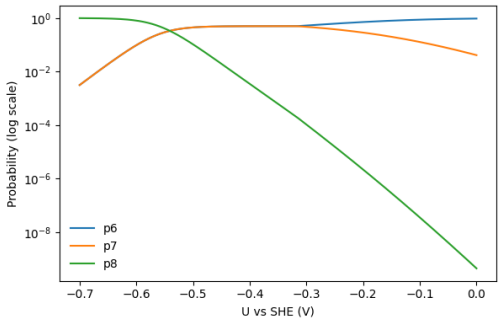

(d)

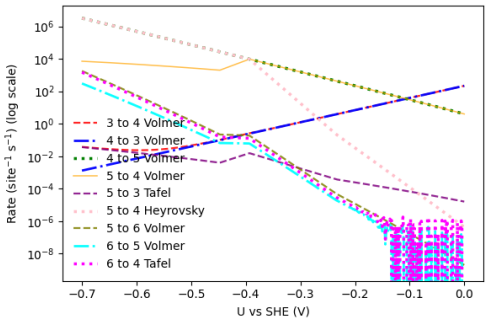

(e)

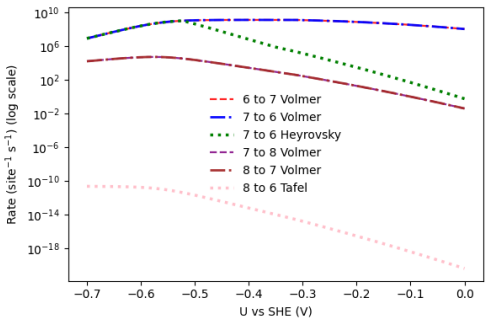

(f)

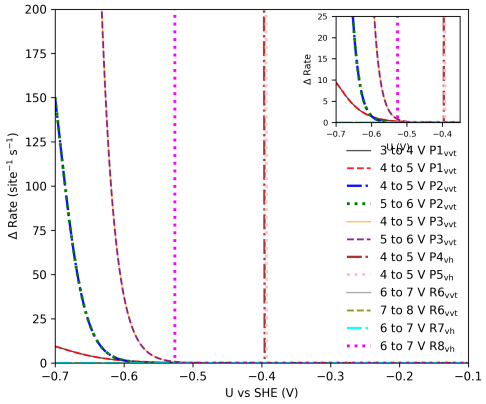

(g)

Figure S23: MKM results for the full network of reaction cycles on pristine (left) and reconstructed (right) surfaces. Panels (a, b) show the rate constants, (c, d) the probability pn of each nH surface state, and (e, f) the overall reaction rates. Panel (g) presents the difference between the forward and backward Volmer step rates across all explored cycles, isolating the current contribution from Volmer steps relative to the Heyrovsky steps.

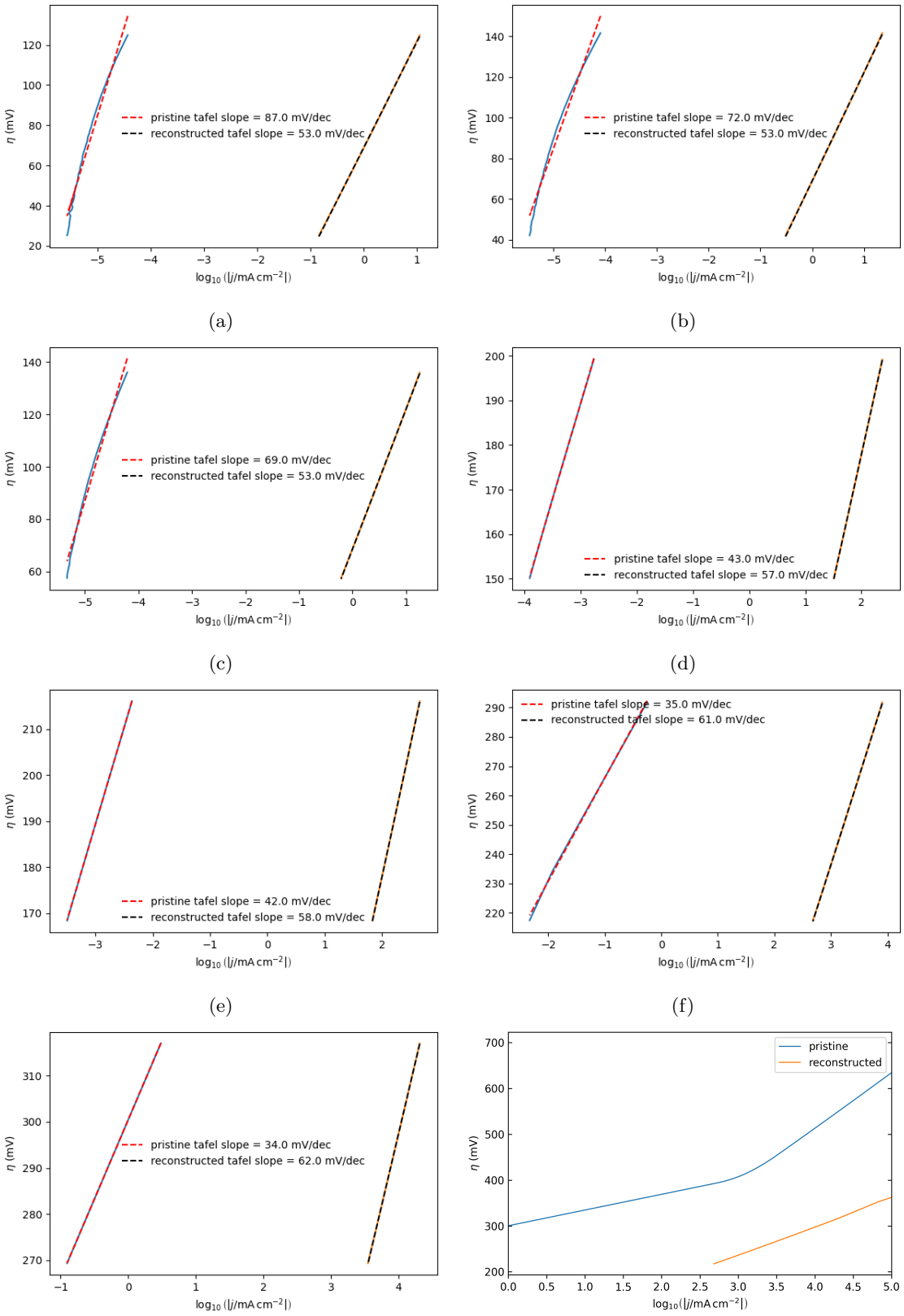

Figure S24: HER Tafel plots across different overpotential (η) regions for pristine (Ni_3P_2) and reconstructed (Ni_3P_2+P) $Ni_2P(001)$ surfaces. Plots (b, e) correspond to low and high ranges from [13], and (f, h) to those from [14]. The pristine surface in (h) qualitatively reproduces the trend reported in [14].

References

[1] K. Mathew, R. Sundararaman, K. Letchworth-Weaver, T. Arias and R. G. Hennig, *The Journal of chemical physics*, 2014, **140**, 084106.

[2] K. Mathew, V. Kolluru, S. Mula, S. N. Steinmann and R. G. Hennig, *The Journal of chemical physics*, 2019, **151**, 234101.

[3] E. Santos and W. Schmickler, *Chemical physics letters*, 2004, **400**, 26–29.

[4] M. Van den Bossche, E. Skúlason, C. Rose-Petruck and H. Jónsson, *The Journal of Physical Chemistry C*, 2019, **123**, 4116–4124.

[5] K. Mathew, V. S. C. Kolluru and R. G. Hennig, *VASPsol: Implicit solvation and electrolyte model for density-functional theory*, https://github.com/henniggroup/VASPsol, 2018, `https://github.com/henniggroup/VASPsol`.

[6] K. Chan and J. K. Nørskov, *The journal of physical chemistry letters*, 2015, **6**, 2663–2668.

[7] S. Ø. Hanslin, H. Jónsson and J. Akola, *ChemPhysChem*, 2024, **25**, e202400349.

[8] L. Xiong, B. Wang, H. Cai, H. Hao, J. Li, T. Yang and S. Yang, *Applied Catalysis B: Environmental*, 2021, **295**, 120283.

[9] S. D. Ghadge, O. I. Velikokhatnyi, M. K. Datta, P. M. Shanthi and P. N. Kumta, *Catalysis Science & Technology*, 2021, **11**, 861–873.

[10] J. O. Bockris, A. K. Reddy and M. Gamboa-Aldeco, *Modern electrochemistry 2A: fundamentals of electrodics*, Springer, 2000.

[11] A. McAuley, *Converting Reference Electrode Potentials*, `https://mcauleygroup.net/article/1/`, 2023, Accessed: 30 October 2025.

[12] H. Sippola and P. Taskinen, *Journal of Chemical & Engineering Data*, 2014, **59**, 2389–2407.

[13] E. J. Popczun, J. R. McKone, C. G. Read, A. J. Biacchi, A. M. Wiltrout, N. S. Lewis and R. E. Schaak, *Journal of the American Chemical Society*, 2013, **135**, 9267–9270.

[14] S. Kong, D. Raturi, B. Owens-Baird, W. Zheng, Y. V. Kolen'ko, P. Singh, D. D. Johnson and K. Kovnir, *ACS Catalysis*, 0, **0**, 18723–18737.